

# MODELING OF SECONDARY RADIATION DAMAGE IN LIGA PMMA RESIST EXPOSURE

Aili Ting  
Sandia National Laboratories  
Livermore, California 94551-0969

## ABSTRACT

Secondary radiation during LIGA<sup>1</sup> PMMA<sup>2</sup> resist exposure adversely affects feature definition, sidewall taper and overall sidewall offset. Additionally, it can degrade the resist adjacent to the substrate, leading to the loss of free-standing features through undercutting during resist development or through mechanical failure of the degraded material. The source of this radiation includes photoelectrons, Auger electrons, fluorescence photons, etc. Sandia's Integrated Tiger Series (ITS), a coupled electron/photon Monte Carlo transport code, was used to compute dose profiles within 1 to 2 microns of the absorber edge and near the interface of the resist with a metallized substrate. The difficulty of sub-micron resolution requirement was overcome by solving a few local problems having carefully designed micron-scale geometries. The results indicate a 2- $\mu\text{m}$  dose transition region near the absorber edge resulting from PMMA's photoelectrons. This region leads to sidewall offset and to tapered sidewalls following resist development. The results also show a dose boundary layer of around 1  $\mu\text{m}$  near the substrate interface due to electrons emitted from the substrate metallization layer. The maximum dose at the resist bottom under the absorber can be very high and can lead to feature loss during development. This model was also used to investigate those resist doses resulting from multi-layer substrate.

**Keywords:** LIGA, resist exposure, secondary radiation damage, undercutting, substrate metallization.

## 1. INTRODUCTION

During LIGA PMMA resist exposure, secondary radiation leads to unwanted doses under the mask absorber. This leads to features having rounded corners and tapered sidewalls. Secondary radiation may also give rise to large doses in masked portions of the PMMA adjacent to the conductive substrate. This may lead to undercutting of features near the substrate, yielding dimensional errors and perhaps the complete loss of some fine features. In addition to undercutting, this secondary radiation near the substrate may degrade the mechanical strength of the PMMA, leading directly to loss of features following complete development. These various concerns are illustrated in Figure 1.

Secondary radiation redistributes the absorbed primary energy. When a photoelectric absorption takes place at a material atomic shell, a photoelectron is emitted, carrying the excess energy that a source photon has above the shell binding energy. Meanwhile, a series of Auger electrons and/or fluorescence photons are emitted during the atom's cascading relaxation. Primary absorption only considers photon energy deposition at its absorption length. As the result, the energy deposition profiles are reasonably uniform in the bulk volume of the resist, but the doses are discontinuous across any material boundary. In fact, photoelectric absorption is eventually realized through electron energy deposition, while any fluorescence photon carrying its unique energy is acting in the same manner as a source photon to produce electrons. Due to the varied directions and very small penetration lengths of electrons, the absorbed energy from a photon is spread around and transits smoothly in a

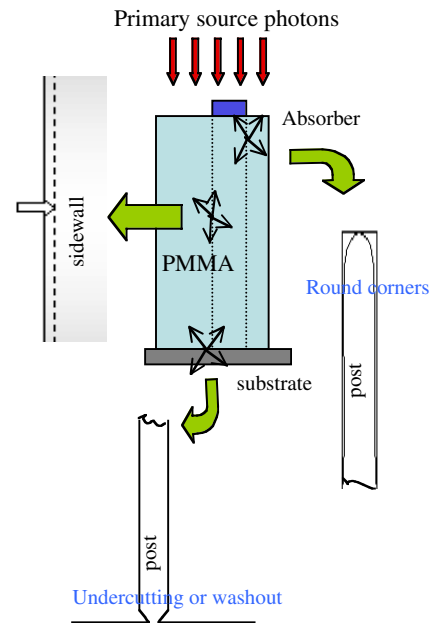


Figure 1. Secondary Radiation

<sup>1</sup> LIGA (Lithographie, Galvanotormung, Abformung in German) means lithography, electroplating, and molding.

<sup>2</sup> PMMA: Polymethyl-methacrylate.

very thin layer near a boundary. Therefore, secondary radiation redistributes the primary absorption dose; it does not superpose on the primary dose.

Secondary radiation includes photon secondaries and electron secondaries. Photon secondaries consist of radiation from photoelectrons, Auger electrons, fluorescence x-ray, and recoil electrons (in photon Compton scattering events); while electron secondaries are radiation from electrons and photons resulting from scattering of electrons. In LIGA exposures the energy source is incident x-ray photons, so photon secondaries are the major secondary radiation; electron secondaries are higher order radiation.

Table 1 shows how an incident photon of 10 keV is absorbed in a photoelectric event, dividing its energy into photoelectron, Auger electrons and fluorescence photons for a few materials of interest. Here, probabilities of Auger electrons and fluorescence photons have been included in the shell binding energy deposition statistical data. The shell binding energy column is equal to the sum of the next three columns: x-ray fluorescence, Auger electrons and local deposition. The primary absorption is simply the incident 10 keV, the sum of the shell binding energy and the photoelectron energy (the second and the last columns), depositing locally, while the secondary radiation absorption (the third to the last columns) deposit to separate places with different penetration lengths and orientations. Note that the local deposition, describing the deposition of the rest energy at the atomic outermost shell at the end of the relaxation process or at the cut-off photon energy, has very small percentage of the binding-energy. Unlike Auger electrons and fluorescence photons, photoelectrons carry energies limited only by incident photon energy that is higher than shell binding energy. Auger electrons generally deposit more energy than fluorescence photons do for materials with  $Z \leq 30$ , since an Auger electron has a greater probability than a fluorescence photon at each atomic shell. For a given source photon energy, K-shell photoelectrons from low-Z materials have stronger energies than from high-Z materials. Thus, for 10 keV source photons, K- photoelectrons deposit much larger energies than Auger electrons except for Cu K-shell absorption, where the large portion of energy is deposited by Auger electrons.

Table 1. Distribution of Shell Binding Energies in a 10-keV Photon Absorption Event  
(Data from EADL —Evaluated Atomic Data Library of LLNL<sup>(1)</sup>)

Atomic Shell	Shell Binding Energy	X-ray Fluorence Lines		Auger Electrons		Local Deposition		Photoelecron Due to a 10 keV Source Photon
		Eng(keV)	%	Eng(keV)	%	Eng(keV)	%	
C(K-)	0.291	0.00047	0.16	0.262	90	0.029	10	9.71
O(K-)	0.537	0.00299	0.56	0.495	92	0.039	7.3	9.46
Al (K-)	1.549	0.055	3.5	1.46	94	0.035	2	8.44
Si (K-)	1.828	0.083	4.5	1.705	93	0.040	2	8.17
Ti (K-)	4.940	0.966	19.6	3.915	79	0.060	1	5.06
Cu (K-)	8.943	3.521	39.0	5.372	60	0.050	1	1.06

Carbon and oxygen atoms in PMMA have K-shell binding energies well below 1 keV, so their photoelectrons are strong and become the major secondary radiation sources inside the resist. The fluorescence photons and Auger electrons emitted from the PMMA can be ignored because of their relatively small energies ( $\ll 1$  keV) and small fluorescence yields.

For substrate materials of interest, near the resist bottom boundaries, energy deposited by photoelectrons and/or Auger electrons emitted from the substrate cannot be neglected due to their micron or sub-micron path length. Whether photoelectrons and Auger electrons are important depends on the material. For example, both of them are important for Ti, but Auger electrons are not important for Al, and photoelectrons are not important for Cu. In Table 1, energy deposited by fluorescence photons emitted from Si and Al substrate can be neglected, but that from Cu and Ti may arise in resist bottom provided the substrate is thicker than the penetration lengths. Cu K-fluorescence photons have a penetration length of 18  $\mu\text{m}$  in Cu, but 1.39 mm in PMMA, while Ti K-fluorescence photons have penetration length of 22  $\mu\text{m}$  in Ti, but 0.23 mm in PMMA. Those fluorescence lengths are much longer than the electron penetration lengths at the energy of interest.

Secondary radiation in LIGA resist exposure has been investigated in recent years.<sup>[2-10]</sup> Experimentally, Pantenburg and Mohr<sup>[2]</sup> and Zumaque et al<sup>[3]</sup> have observed 2-10  $\mu\text{m}$  degradation at the top and bottom of resist for tall structures. Pantenburg and Mohr also investigated the correlation between substrate adhesion and absorber height. The simulation work so far has indicated only sub-micron degradation mostly by using varied Monte Carlo methods (MC). Among these simulations, Murata<sup>[4-6]</sup> presented detailed analysis of his MC results for very thin PMMA film under low photon energies. Feldman and Sun<sup>[7]</sup> used a one-dimensional model showing a narrow transition region of 0.1  $\mu\text{m}$  across the absorber inside the resist for low photon energy. Feiertag et al<sup>[8-9]</sup> defined the lateral degradation of about 0.4  $\mu\text{m}$  in PMMA in their MC results as well as from their measurements by using a dissolution limit of 1.8  $\text{kJ}/\text{cm}^3$ . They also computed resist absorption by Ti substrate fluorescence photons. Schmidt et al.<sup>[10]</sup> presented their MC results showing a 1-1.5  $\mu\text{m}$  substrate boundary layer for Cu and Ti substrates attached to a 500- $\mu\text{m}$  resist bottom. Zumaque et al. run a 64-processors parallel computer system to investigate the tall resist structure (750  $\mu\text{m}$ ). Using 5% of the max dose, they defined a lateral degradation at resist bottom of 0.3  $\mu\text{m}$  for a Ti substrate. Their transition region inside the resist was about 2  $\mu\text{m}$  by using 1.5  $\text{kJ}/\text{cm}^3$  as the dissolution limit. However, when lowering the dissolution limit, for example, a 100  $\text{J}/\text{cm}^3$  limit, the degradation will be more severe. Running at workstations, Sandia LIGA exposure models have included photon scattering,<sup>[11]</sup> fluorescence lines<sup>[12-13]</sup>, and photoelectrons,<sup>[14]</sup> but not yet included Auger electrons or included all photons and electrons together, so a modeling software including all photon/electron secondary radiation sources is preferable to investigate the secondary radiation damage under Sandia's LIGA operation conditions.

Therefore, coupling photon/electron transport is a more accurate way to describe the photoelectric absorption, especially, in the tiny area near the absorber edge inside the resist and near the resist bottom interface. Although this is a challenge for problems of LIGA x-ray exposure owing to the required sub-micron resolution, this difficulty is overcome by solving a few local problems having carefully designed micron-scale geometries using Sandia's ITS radiation transport software.<sup>[15-18]</sup> Sub-micron resolution of the dose profiles within 1 to 2 microns of the absorber edge and near the interface of the resist with a metallized substrate were obtained. This model was also used to investigate secondary resist doses resulting from multi-layer substrate. Such a multi-layer scheme enables the use of low-Z metals (aluminum, magnesium, etc.) to provide good electrical conduction and low secondary doses while also providing a good surface metal (titanium, copper, nickel, etc.) for LIGA electrodeposition. We show that the maximum secondary resist dose can be limited by making the surface layer sufficiently thin.

## 2. SAMPLE PROBLEMS AND RESULTS

**SAMPLE PROBLEM 1.** Primary Versus Secondary Radiation Under Au Absorber (10 keV source photons, 4.5 M steps in 20 batches, 3+days). The layout is Si (100- $\mu\text{m}$  thick, 12- $\mu\text{m}$  wide) mask substrate, Au (25- $\mu\text{m}$  thick, 3- $\mu\text{m}$  wide) absorber, PMMA (500- $\mu\text{m}$  thick, 12- $\mu\text{m}$  wide) resist, as in Figure S1-1

The absorption dose distribution over the PMMA width is calculated through 112 tall but narrow grids of the size 0.1- $\mu\text{m}$  by 480- $\mu\text{m}$ . In Figure S1-2, the smooth curve is the energy deposition profile while the jump curve is from the photon- only calculation. The energy deposition by PMMA photoelectrons smoothes the transition across the absorber edge, so the exposure accuracy is thus compromised by unwanted doses within a 2- $\mu\text{m}$  transition region around the absorber edge and from the side. This region thickness is just about the continuous-slowing down approximation (CSDA) range<sup>[15]</sup> of the PMMA electrons at 10 keV.

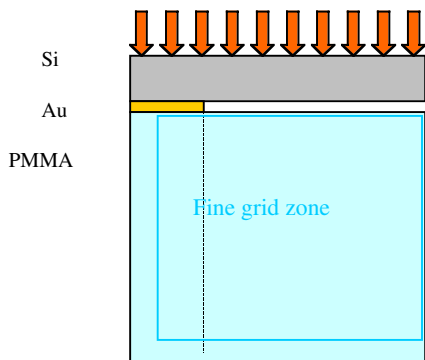


Figure S1-1

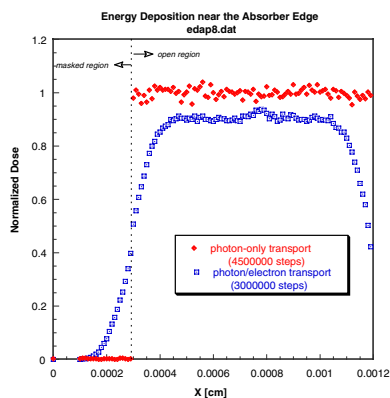


Figure S1-2

**SAMPLE PROBLEM 2.** Estimation of PMMA Bottom Doses For Cu-Si Substrate (10 keV source photons, 100 M steps in 20 batches, 6 days). The layout is Si (100- $\mu\text{m}$  thick, 16- $\mu\text{m}$  wide), Au (25- $\mu\text{m}$  thick, 8- $\mu\text{m}$  wide), PMMA (500- $\mu\text{m}$  thick, 16- $\mu\text{m}$  wide), Cu (0.5- $\mu\text{m}$  thick, 16- $\mu\text{m}$  wide), Si (5- $\mu\text{m}$  thick, 16- $\mu\text{m}$  wide), as in Figure S2-1.

The vertical absorption dose distribution at the resist bottom under absorber is calculated through 30 short but wide fine grids of the size 0.1- $\mu\text{m}$  by 2- $\mu\text{m}$ . Figure S2-2 gives the dose profile in the fine grid zone of Figure S2-1, The two curves (for 3 and 100 million steps) have the same trend, although the one with only 3-million steps fluctuates more. A one- $\mu\text{m}$  dose boundary layer from the resist bottom receives significant absorption that cannot be ignored. At the resist bottom, the dose is about 30 times of the average dose (reference value). Hence, under the absorber, the secondary absorption in this bottom dose boundary layer has a very steep profile and the bottom dose may attack the adhesion between the resist and the substrate.

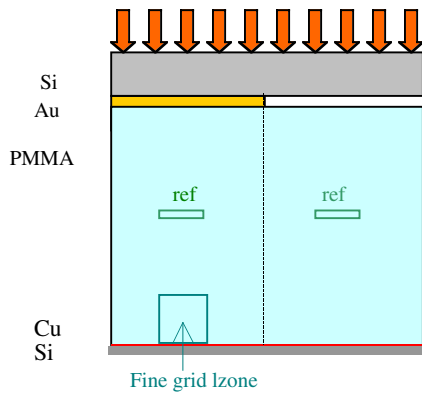


Figure S2-1

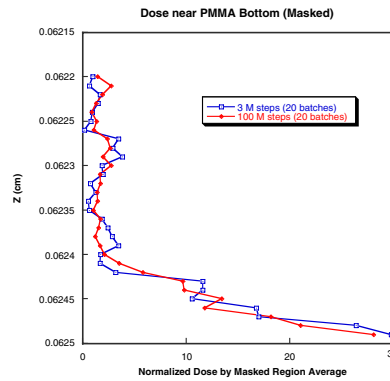


Figure S2-2

**SAMPLE PROBLEM 3 (Series).** Examination of Substrate Materials on PMMA Washout (5-20 keV source photons, single or double layer substrates). The layout is PMMA (7  $\mu\text{m}$  thick, 11  $\mu\text{m}$  wide), substrate (varied 0.1–5  $\mu\text{m}$  thick, 11  $\mu\text{m}$  wide), as in Figure S3-1

To greatly shorten the time for each run, different substrate materials are computed in the resist open region comparing with a Cu substrate, which resist bottom dose under the absorber is known in previous sample problem. Thus, a much shorter height in the open region is adopted, and only two materials (resist and substrate) are selected. The vertical absorbed dose distribution is calculated through 20 short but wide grids of the size 0.1- $\mu\text{m}$  by 5- $\mu\text{m}$ .

The twelve calculated cases are the following: PMMA (5- $\mu\text{m}$ ) substrate, (10 keV, 2M steps–20 batches), Cu (5- $\mu\text{m}$ ) substrate, (10 keV, 1M steps–20 batches), Ti (5- $\mu\text{m}$ ) substrate, (10 keV, 6M steps–20 batches), Al (5- $\mu\text{m}$ ) substrate, (10 keV, 6M steps–20 batches), Cu (0.5- $\mu\text{m}$ ) substrate, (10 keV, 3M steps–20 batches), Cu (5- $\mu\text{m}$ ) substrate, (5 keV, 1M steps–20 batches), Cu (5- $\mu\text{m}$ ) substrate, (20 keV, 10M steps–20 batches), Ti (.1- $\mu\text{m}$ ) substrate, (10 keV, 6M steps–20 batches), Ti (.1)-Cu (.4) substrate, (10 keV, 2M steps–20 batches), Ti (.1)-Al (.4) substrate, (10 keV, 6M steps–20 batches), Ti (.01)-Cu (.4) substrate, (10 keV, 10M steps–20 batches), Ti (.01) Al (.4) substrate, (10 keV, 10M steps–20 batches). These calculations enable us to do comparisons for substrate material and thickness, source photon energy, and single or multi-layer substrate. The statistic of the secondary radiation sources is also discussed.

The results.

(1) Absorption Dose Profiles in Resist Bottom Boundary Layer

Figure S3-2 shows the absorption dose profile in a 2- $\mu\text{m}$  height from resist bottom for all cases. PMMA substrate is used as a reference, since the dose will be uniform. The dose profiles in the resist bottom boundary layer are caused by the substrate electrons and fluorescence. The thickness of the bottom boundary layer is around 1 $\mu\text{m}$  at 10 keV (but about 1.5  $\mu\text{m}$  and 0.4  $\mu\text{m}$  for Cu at 20 keV and 5 keV, respectively) that is approximately proportional to the CSDA range of the substrate material at the same energy. The exception is the Ti (0.1), the profile of which is uniform since the 0.1- $\mu\text{m}$  Ti substrate is too thin to produce any significant photoelectrons and Auger electrons.

(2) Effect of Atomic Numbers of Substrate Materials

Comparing 5- $\mu\text{m}$  substrates of Cu, Ti, Al, and PMMA at 10 keV, the absorption doses at the resist bottom for the four are decreasing (20, 14 and 4 times of average open dose) according their descending atomic numbers

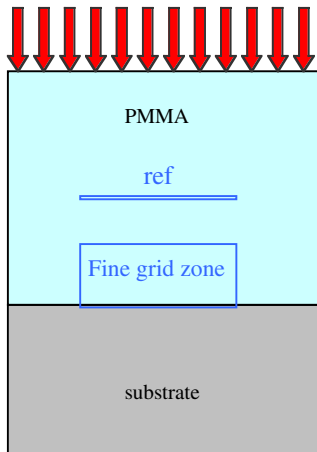


Figure S3-1

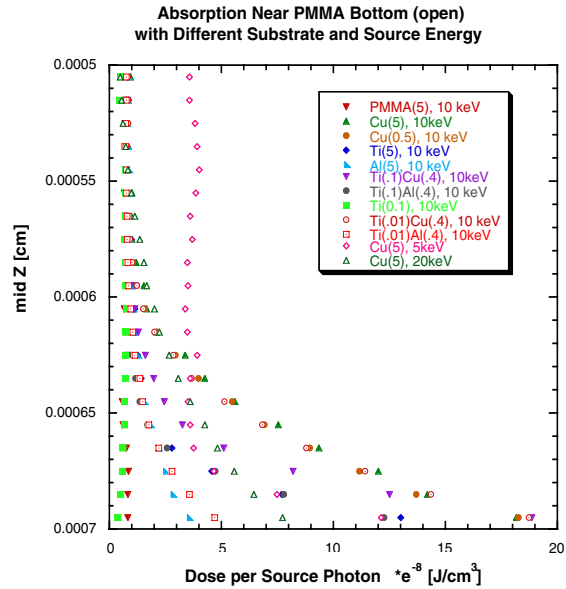


Figure S3-2

(3) Advantage of Extremely Thin Ti Top Layer in Multi-layer Substrate.

The cases of 0.01 $\mu\text{m}$  of Ti top substrate layer (attached on Cu or Al) make no essential difference in the profile from the case without Ti, while the case of 0.1 $\mu\text{m}$  Ti top substrate layer make moderate differences. This result suggests thin Ti can be selected over other materials in multi-layer substrate for designing resist substrate metalization. Such a multi-layer scheme enables the use of low-z metals (such as Al) to provide good electrical conduction and low secondary doses while also providing a good surface metal for LIGA electrodeposition.

(4) Effect of The Thickness of Cu Substrate

In Figure S3-2, the dose boundary profiles at the resist bottom for all sample problems with Cu substrate are very similar because the CSDA range of Cu at 10 keV is about 0.5  $\mu\text{m}$ . Therefore, a 5- $\mu\text{m}$  Cu substrate reabsorbs its own secondary absorption inside the substrate at locations 0.5  $\mu\text{m}$  farther from the resist bottom, so only the secondary radiation generated at the top 0.5  $\mu\text{m}$  layer of Cu can reach the resist bottom.

(5) Influence of Source Photon Energy

A 5- $\mu\text{m}$  Cu substrate at three different source photon energies is compared. In Figure S3-2, the largest absorption at the resist bottom is 10-keV case, followed by 5-keV and 20-keV cases. The lowest absorption case is for 20-keV case since the CSDA range of Cu at 20 keV is about 3 times longer than at 10 keV. On the other hand, at 5 keV, no K-shell absorption (only L-shell and below) for Cu will happen, so the absorption is more in the long wavelength energy range that produces lesser dose. Although the average open resist dose at 5 keV is greater than all the cases, it does not result from the substrate. Since the CSDA range of PMMA at 5 keV is about three times shorter than at 10 keV, the average open dose is also three times larger.

STATISTICS OF THE SECONDARY RADIATION SOURCES

(1) The Number Ratio of Penetrated Source Photons

Figure S3-3 presents the penetrating source photons ratios. The greater the penetration of the source photons, the less the source photons will interact with the material atoms, and less absorption will result. The least penetrated case is 40% of the source photons for the 5- $\mu\text{m}$  Cu substrate at 10 keV and 5 keV. This means that as many as about 60% source photons interact with the resist to produce absorption because the 10 keV of the source photons is close to Cu's K-shell binding energy and the 5 keV is also not very far from Cu's L-shell binding energy.

At 10 keV, the most penetrated cases are 99.5%, 99.4%, 99.2%, 98.9%, and 96.2% for substrates PMMA, Ti (0.01)-Al (0.4), Ti (0.1), Ti (0.1)-Al (0.4), and Al (5), respectively, so only 0.5 to 3.8% source photons interact with the resist. This is because the K-shell binding energies for those materials are low (below the ITS cut-off energy 1 keV for C and O in PMMA, and about 1.8 keV for Al). Although Ti's K-shell energy is about 4.9 keV, there are not enough Ti atoms to excite for very thin Ti layer. In contrary, penetrated source photons in Ti (5) are 77.7%, which allows a larger absorption. Also note that the ratio of penetration is about 87% for Cu (5) at 20 keV due to the long CSDA range.

(2) Total Energy Deposited by Each Radiation Source.

Figure S3-4 shows the total energy deposited by each secondary radiation source for the resist with a 5- $\mu\text{m}$  substrate of Cu, Ti, Al, and PMMA, respectively, using a 10 keV source. Note that the high-order contributions from Compton recoil electrons, Bremsstrahlung photons (electron secondaries) and fluorescence photons that originated from electrons are negligible because they are negligible.

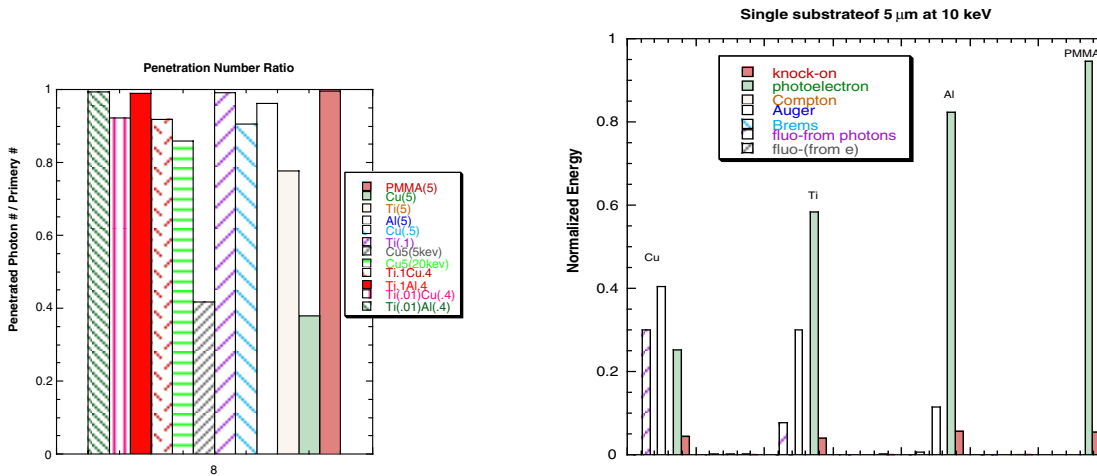


Figure S3-3 Penetration Number Ratio

Figure S3-4 Deposited Energy by Sources (5- $\mu\text{m}$  Substrate at 10 keV)

Contributions from photoelectrons are 89%, 82%, and 58% for PMMA, Al, and Ti substrates, respectively, dominating in all cases except for the Cu substrate (25%) because photoelectrons emitted from Cu are relatively weak (1.1 keV) for 10 keV source. Photoelectrons emitted from C and O in PMMA are the strongest (10 keV) since the K-shell binding energy of C and O are below 1 keV (ITS cut-off at 1 keV). Photoelectrons emitted from Al are about 8.4 keV, and from Ti are about 5.1 keV.

There are no Auger electrons for the PMMA substrate since their energies are below 1 keV, while they are the most important radiation source for the Cu substrate (40%), followed the Ti substrate (30%). However, they contribute only 12% for the Al substrate since the Al K-shell binding energy is low.

Fluorescence photons that result from source photons contribute 30% for the Cu substrate. Their contributions are more important than the photoelectrons because the high K-shell binding energy. However, fluorescence photons contribute only 8% for Ti substrate since the K-fluorescence yield (about 0.21) is small, and can be ignored for Al and PMMA substrates.

Contribution from knock-on (electron scattering) is generally small (about 5%) because the incident source is photon, but much greater than that from Compton, Bremsstrahlung, and fluorescence originated from electrons. Contributions from knock-on electrons are mainly from PMMA photoelectrons and are comparable with that from Auger electrons for Al substrate, and with that from fluorescence photons for Ti substrate.

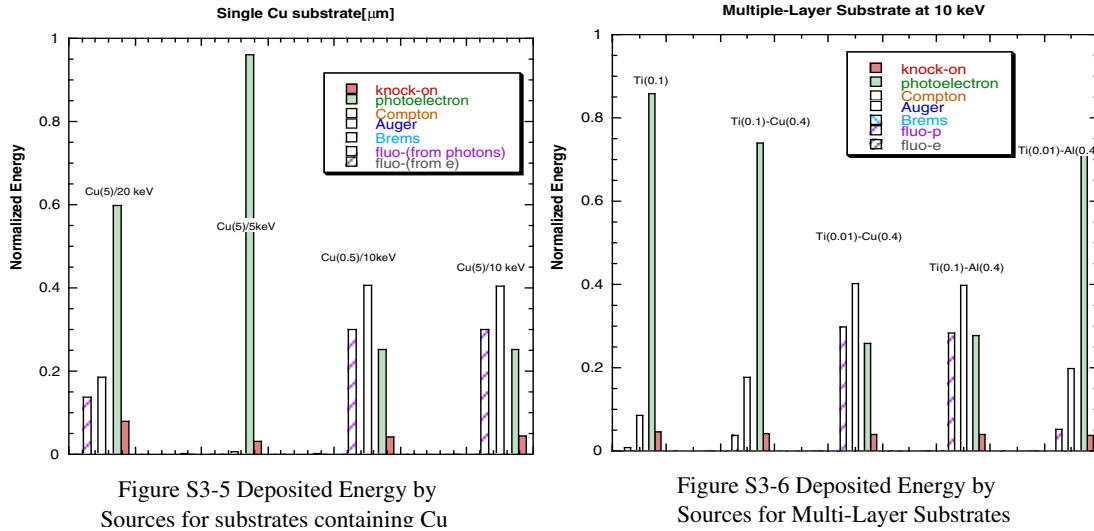
(3) Total Energy Deposited by Each Radiation Sources for Substrates Containing Cu

Figure S3-5 shows total energy deposited by sources for Cu (5  $\mu\text{m}$ ) and Cu (0.5  $\mu\text{m}$ ) at 10 keV, and Cu (5  $\mu\text{m}$ ) at 5 keV and 20 keV. The energy distribution for Cu (5) and Cu (0.5) at 10 keV are similar, as far as the thickness is no less than the electron CSDA range at 10 keV. Auger electrons deposit the most (40%), followed by fluorescence (30%), and

photoelectrons (25%). However, for varied photon energy sources, the deposited energy percentage by each source can be very different. For 5 keV case, the photoelectrons are dominant, contributing above 95% of the total energy since fluorescence photons and Auger electrons are produced by the L-shells and below and have even smaller contribution than the knock-on. For the 20 keV case, high-energy source photons produce very high-energy photoelectrons (about 11.1 keV), (which also induce about 8% knock on contribution), so it deposits above 95% of the total energy, followed by Auger electrons (about 18%), and by fluorescence (about 14%).

(4). Total Energy Deposited by Each Source for Multi-Layer Substrates.

Figure S3-6 shows the energy deposited by each source for multi-layer substrates at 10 keV source. The substrates are Ti (0.1)-Cu (0.4), Ti (0.01)-Cu (0.4), Ti (0.1)-Al (0.4), and Ti (0.01)-Al (0.4). Ti (0.1) is also plotted for comparison.



Comparing with Figure S3-4, the energy distribution for substrate Ti (0.01)-Cu (0.4) is almost the same as that for Cu (0.5), and the energy distribution for substrate Ti (0.01)-Al (0.4) is similar to that for Al (5). However, the energy distribution for substrate Ti (0.1)-Cu (0.4) is not similar to Cu (0.5) but is close to Ti (0.1). The energy distribution for substrate Ti (0.1)- Al (0.4) is not similar to that for Al (5), nor to that for Ti (0.1). Therefore, a sufficiently thin good surface metal, like a 0.01- $\mu\text{m}$  Ti, does not change essentially the deposited energy distribution. Together with Figure S3-2, this thin layer does not produce extra dose at the resist bottom.

(5) Escaped energies

The number ratio of escaped photons and electrons are shown in Figure S3-7, respectively. Among them, only Cu (5) at 10 keV is the one that escapes 18% of photons and escapes the most energy. Although the number ratio of penetrated photons in Cu (5) at 10 keV is only 40% (Figure S3-3), the large number of escape makes the Cu (5) at 10 keV not very different from other cases containing Cu in knock-on energy, Auger energy, Compton energy, Bresstrahlung energy, etc., except in photoelectron energy for Cu (5) case at 20 keV

(6) Absorption in the Substrates

A part of the total deposited energy is absorbed in the substrate. The higher the absorption in the substrate, the less efficiency of source energy will result. High doses produces high temperature in the metal, which may induce some unwanted effects to the resist. Absorptions in the substrates including the top layer and the second layer are shown in Figure S3-8. As expected, PMMA substrate has no absorption above 1 keV that is the cut-off energy in the method. Again, substrates with Cu absorbs the most at 10 keV no matter if it is a single substrate or the second layer of the substrate, since its K- shell binding energy is the highest among all of the materials here. Cu (0.5) and the second layer Cu (0.4) absorb the most because lesser escape than Cu (5) at 10 keV (Figure S3-7). Cu at 20 keV is penetrated by 87% source photons and at 5 keV absorbs only in L-shells and below, so they have less absorption.

**SAMPLE PROBLEM 4-1.** Two-Dimensional Calculation to Examine PMMA Undercutting for Cu-Si substrate. (10 keV source photons, 40 M steps in 20 batches). The layout is Au (25- $\mu\text{m}$  thick, 4- $\mu\text{m}$  wide), PMMA (500- $\mu\text{m}$  thick, 11- $\mu\text{m}$

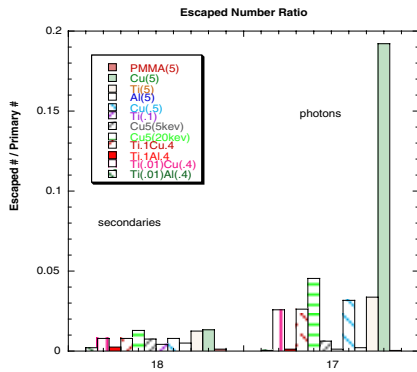


Figure S3-7 Escaped Number Ratio

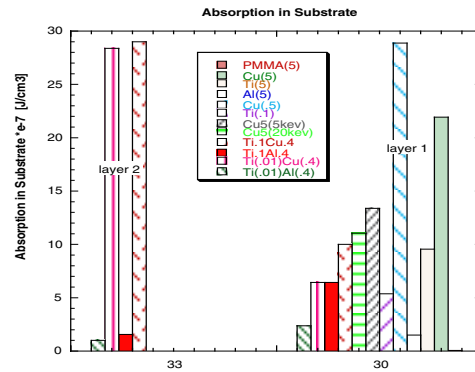


Figure S3-8 Absorption in Substrates

wide), Cu (0.5- $\mu\text{m}$  thick, 14- $\mu\text{m}$  wide, extend beyond PMMA), Si (5- $\mu\text{m}$  thick, 14- $\mu\text{m}$  wide, extend beyond PMMA), as in Figure S4-11.

The two-dimensional absorption dose profile in a rectangular region of 2- $\mu\text{m}$  by 1- $\mu\text{m}$  at the PMMA bottom with one half zone under the absorber was calculated through 50 square fine grids of 0.2- $\mu\text{m}$  by 0.2- $\mu\text{m}$  as shown in Figure S4-11.

**The results.** Figure S4-12 gives a contour plot of the two-dimensional doses in the fine grid zone of Figure S4-11. Figure S4-13 gives the dose curves along five horizontal grid lines (from top to bottom correspond to horizontal grid lines from bottom to top). The average dose line of the open region is plotted, so all data points above this line in Figure S4-13 have the doses greater than the average open dose. Under the absorber, a curved triangle region about 0.8  $\mu\text{m}$  height from bottom and 0.5  $\mu\text{m}$  width from the corner having absorption above the average open dose can be observed. This agrees with observation from Figure S4-12.

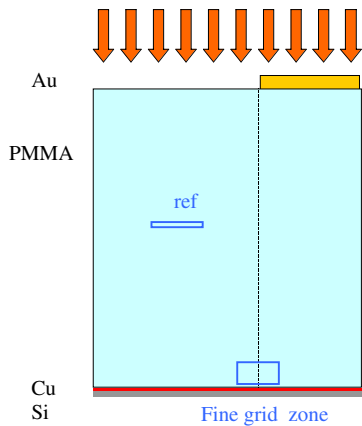


Figure S4-11

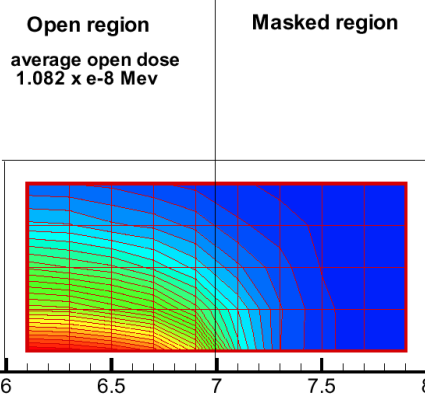


Figure S4-12

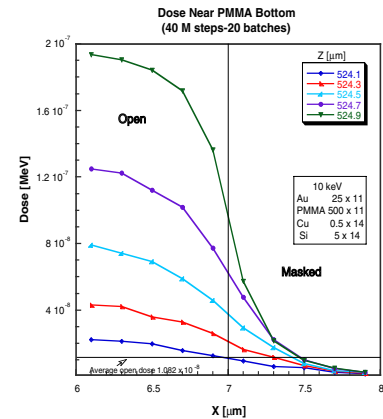


Figure S4-13

Under the absorber, the max dose at the bottom corner is about 12 times of the average open dose, while the max dose at the bottom corner of the open region is about 20 times of the average dose, as indicated in previous sample problems.

**SAMPLE PROBLEM 4-2.**

This problem has the same layout and the fine grid zone as the problem 4-1, but with a top Al substrate layer instead of Cu. Due to more Auger electrons generated in Al than Cu, this calculation is more difficult to converge,

The results. Figure S4-22 is the dose contour plot of the fine grid zone, in which the bottom corner dose under the absorber is about 2.1 times of the average open dose. Comparing with the results in Figure S4-13, the triangular region whose dose is above the average open dose is much smaller (about  $0.5 \mu\text{m}$  vertically by  $0.3 \mu\text{m}$  horizontally), since Al has a lower atomic number than Cu.

Figure S4-23 compares the surface plots of the sample problems 4-1 and 4-2 with the same scale. The results show that the doses in the resist for Cu are about five times larger than that for Al, thus, Al is a better substrate than Cu.

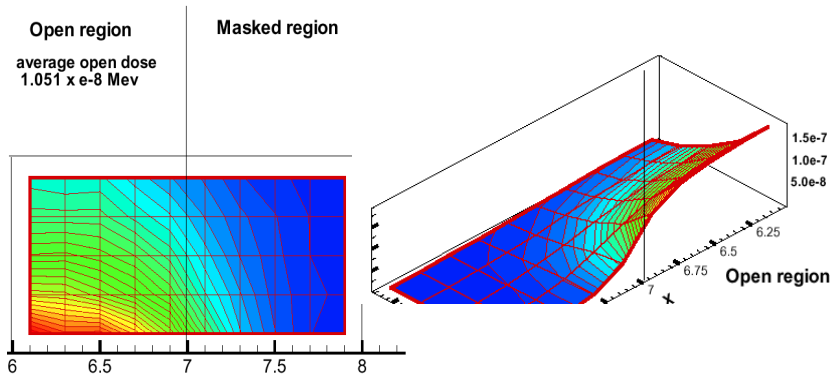


Figure S4-22

SAMPLE PROBLEM 5-1 (Series). Determining Thickness of Ti for Ti-Al (0.4) Substrate Under Different Source Photon Energy. (Ti from  $0.005$  to  $1 \mu\text{m}$  for 5, 10, and 20 keV, 3-20 M steps in 20 batches). The layout is PMMA ( $7 \mu\text{m}$  thick,  $11 \mu\text{m}$  wide), Ti (varied  $0.005$ – $1 \mu\text{m}$  thick,  $11 \mu\text{m}$  wide), Al ( $0.4 \mu\text{m}$  thick,  $11 \mu\text{m}$  wide), optional Si ( $10 \mu\text{m}$  thick,  $11 \mu\text{m}$  wide) as in Figure S5-11.

By selecting simple layout and shorter heights in the open region, the bottom absorption dose distributions are calculated through only two short but wide fine grids ( $0.1\text{-}\mu\text{m}$  by  $5\text{-}\mu\text{m}$ ) to shorten the runtimes. The source photon energy of 5, 10, 15, and 20 keV are used to compare the results.

The results. It can be seen in Figure S5-12 that there is a transition region of Ti thickness over which the dose absorbed at the resist bottom increases about three times for all source photon energy cases. The most obvious case involves 5-keV source photon energy, which has the highest dose among the source photon energies, so the enhanced dose becomes very high. On the other hand, in the case with 20 keV, the dose at any thickness is at least 10 times smaller than that with 5 keV.

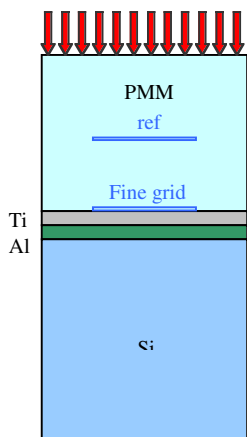


Figure S5-11

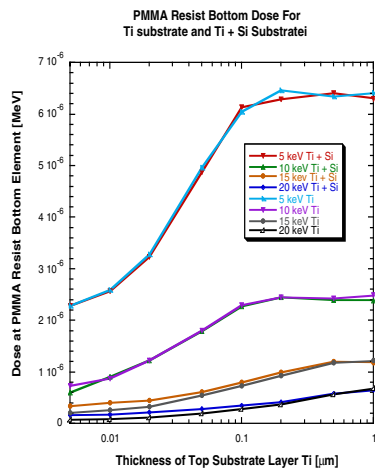


Figure S5-12